Sensors and Actuators

Contents lists available at ScienceDirect

Sensors and Actuators A: Physical

journal homepage: www.elsevier.com/locate/sna

Electromechanical characterization of a 3D printed dielectric material for dielectric electroactive polymer actuators

David Gonzalez[a], Jose Garcia[a], Brittany Newell[a*]

[a] School of Engineering Technology, Purdue University. Adaptative Additive Technologies Lab.

ARTICLE INFO

Article history:
Received
Received in revised form
Accepted
Available online

Keywords:
Dielectric
Electroactive polymer
3D Printing
Dielectric constant
Actuator
Pre-strain

ABSTRACT

Dielectric electroactive polymers (DEAPs) represent a subclass of smart materials that are capable of converting between electrical and mechanical energy. These materials can be used as energy harvesters, sensors, and actuators. However, current production and testing of these devices is limited and requires multiple step processes for fabrication. This paper presents an alternate production method via 3D printing using Thermoplastic Polyurethane (TPU) as a dielectric elastomer. This study provides electromechanical characterization of flexible dielectric films produced by additive manufacturing and demonstrates their use as DEAP actuators. The dielectric material characterization of TPU includes: measurement of the dielectric constant, percentage radial elongation, tensile properties, pre-strain effects on actuation, surface topography, and measured actuation under high voltage. The results demonstrated a high dielectric constant and ideal elongation performance for this material, making the material suitable for use as a DEAP actuator. In addition, it was experimentally determined that the tensile properties of the material depend on the printing angle and thickness of the samples thereby making these properties controllable using 3D printing. Using surface topography, it was possible to analyze how the printing path affects the roughness of the films and consequently affects the voltage breakdown of the structure and creates preferential deformation directions. Actuators produced with concentric circle paths produced an area expansion of 4.73% uniformly in all directions. Actuators produced with line paths produced an area expansion of 5.71% in the direction where the printed lines are parallel to the deformation direction, and 4.91% in the direction where the printed lines are perpendicular to the deformation direction.

1. Introduction

For the past three decades, polymer materials have been investigated and characterized through analysis of their mechanical or electrical response when they are exposed to electric, chemical, pressure, optical, or magnetic fields; finding some correlation or influence of the external stimulus on their electromechanical properties. Smart polymers are defined as materials that respond to a stimulus, and they have been investigated and used in numerous inventions over the past few decades. Electroactive polymers represent one group of these materials [1]. Electroactive polymers are structures that can change in size and shape when exposed to an electric field. Electroactive polymer structures are also capable of converting mechanical strain into electrical signals, making them attractive and useful for sensors and energy harvesting. These materials are generally classified in two sub-classes: electronic and ionic [2]. Electronic EAPs are activated by electrostatic forces that are produced when a polymer film is placed between two electrodes. The strains seen in this type of material can be caused by the described Coulomb forces and electrostriction. In addition, electronic EAP's generally require high voltages (1 – 10 kV) to be actuated but present very low electrical power consumption using only 100 – 2000 microamps of current, and their response time is in the millisecond range. On the other hand, ionic EAPs are activated by transport or diffusion of ions inside the polymer when it is placed between two electrodes. These materials operate in a wet state or in solid electrolytes. Ionic EAPs usually require low voltages (1 – 10 V) [3].

Each of these types of electroactive polymers has its advantages and disadvantages and should therefore be selected based on end application. The electronic EAP materials are often more favorable for applications of structural analysis and mechanical systems, due to their high mechanical energy density and fast response. On the other hand, ionic materials are

* Corresponding author.
E-mail address: gonza476@purdue.edu (D. Gonzalez), jmgarcia@purdue.edu (J. Garcia), bnewell@purdue.edu (B. Newell).

often more favorable for biomedical applications due to the aqueous environment for application and the ability to actuate at low voltages [4].

Dielectric electroactive polymers are materials with high dielectric breakdown strength and low elastic stiffness and are used in electroactive structures such as electrical insulators. The dielectric material is polarized when it is placed between two electrodes and an electrical field is induced between them. The electric stimulus creates a mechanical displacement between the electrodes generating a compression in the thickness of the elastomer film and an expansion in the active area covered by the electrodes for volume to be conserved [5]. This electroactive structure can be represented by a parallel plate capacitor as shown in figure 1 and can be modeled using equation 1. Based on equation 1, an ideal dielectric material must have high relative permittivity and a small thickness to increase the equivalent pressure experienced by the elastomer film when exposed to an electric field.

$$P_{equivalent} = \varepsilon_0 * \varepsilon_r * \left(\frac{U}{d}\right)^2 \qquad (1)$$

$P_{equivalent}$ = Equivalent pressure

U = Voltage

d =Thickness of the dielectric films

ε_0 = Free space permittivity (8.85 x 10^-12 F/m)

ε_r = Relative permittivity of the dielectric material

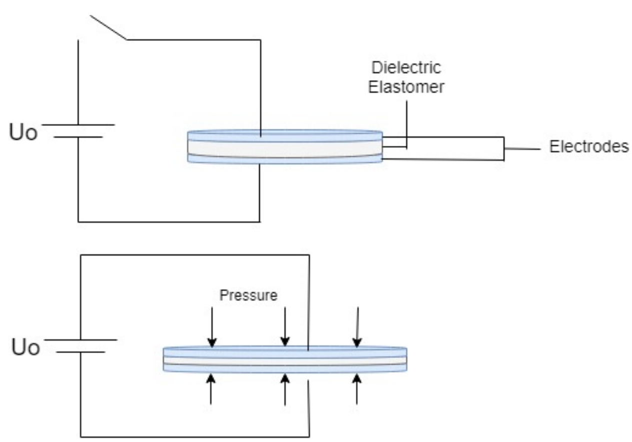

Fig 1. Structure and working principle of soft dielectric EAP.

This type of structure presents two states: polarized and non-polarized. When high voltage is applied, the structure transitions to a polarized state where the dielectric films presents thickness contraction and lateral expansion, where the magnitude and direction of the movement depends on the properties of the dielectric material. As soon as the high voltage is removed the structure returns to its initial non-polarized state. DEAP actuators have two different directions in which the actuation of the structure can be used: the planar direction using the structure as an expanding actuator, or the thickness direction using the structure as a contractile actuator.

2. Manufacturing Process

While numerous patents have been generated using electroactive polymer concepts, few actual products have been realized. Current manufacturing processes for electroactive polymers are generally roll to roll processes or lab-scale procedures. Roll to roll processes make production of variable geometries and conditions burdensome and expensive to complete.

A common method used to increase the actuation of this type of materials is stacking. Hundreds of thin layers of a dielectric elastomer and electrodes can be stacked to form an effective actuator producing higher achievable forces and larger displacements [6-7]. These techniques can be labor intensive using current manufacturing processes. Based on the above, 3D printing techniques were selected to manufacture dielectric elastomers because this technology allows for a reduction in production cost and time while allowing for design and geometry flexibility [8]. Furthermore, the operational foundation of 3D printing is to manufacture a large number of layers continuously, which in this case is useful to produce improved actuators and opens the possibility to create innovative designs.

Fused deposition modeling (FDM) was selected as the manufacturing method based on the available printers, materials, and suitability for electroactive polymer production. This technique uses plastic extrusion with a heated extruder that follows a print path dictated by the desired structure to be printed [9]. The heated extruder uses a simple feeding mechanism based on the friction of small gears, which can be modified to facilitate the printing of flexible materials. In this research a Lulzbot Taz 6 was used to manufacture the dielectric films using a flexible filament and a specialized extruder head with modifications to support higher extrusion temperatures.

3. Dielectric Material

The most common flexible materials available for FDM 3D printing are thermoplastic polyurethanes (TPUs). These materials present an elastic behavior under traction and contractile forces [10]. This type of polymer can be produced with varying elastic properties, which means that is possible to find the same class materials with different stiffness values. The dielectric films used in this research were made using a soft TPU with a Shore A hardness of 60 (Diabase X60 Ultra Flexible Filament). This is currently the softest, most flexible elastic filament available in the market. Printing with this filament can produce finished parts that are highly functional for applications that require stretching and flexibility. In addition, this material is resistant to oil, grease and abrasion, making this material ideal for industrial applications [11].

4. Results (Electromechanical Characterization)

4.1. Permittivity evaluation

Permittivity is a material property that affects the Coulomb force between two point charges in the material and indicates how easily a material can become polarized by imposition of an electric field on an insulator. The dielectric constant (K) is equivalent to the complex relative permittivity (or the complex permittivity (ε^*) relative to the permittivity of free space (ε_0). The real part of complex relative permittivity (ε_r') is a measure of how much energy from an external field is stored in a material; $\varepsilon_r' > 1$ for most solids and liquids. The imaginary part of complex relative permittivity (ε_r'') is called the loss factor and is a measure of how dissipative a material is to an external field. ε_r'' is always > 0 and is usually much smaller than ε_r'. The loss factor includes the effects of both dielectric loss and conductivity [12].

$$K = \varepsilon_r^* = \frac{\varepsilon^*}{\varepsilon_0} = \varepsilon_r' - j\varepsilon_r'' \qquad (2)$$

Based on equations 1 and 2, a good dielectric material for an EAP actuator must have a high relative permittivity value, which will in turn, increase the pressure exerted on the electrodes by the dielectric elastomer. The dielectric test fixture, Agilent 16451B was used to measure the capacitance of different types of 3D printed TPU samples. This equipment is capable of measuring solid materials up to 30 MHz using parallel plates as a measurement method. The parallel plate method, also called the three terminal method in ASTM D150 [13], involves sandwiching a thin sheet of material or liquid between two electrodes to form a capacitor. The measured capacitance is then used to calculate permittivity.

In this test, guard electrodes were used to absorb the electric field at the edges ensuring the capacitance that was measured between the electrodes was only composed of the current that flowed through the dielectric material. Electrode – A (38 mm guard electrode) was selected and used for the test, because this type of electrode is used to measure materials without a thin film electrode. Capacitance was recorded with an Agilent 4263B LCR Meter at 100 kHz. The TPU samples were 3D printed with a circular shape (54 mm outer diameter) and varying the thickness from 1 to 5 mm. Five samples per thickness value were tested, for a total of 25 samples tested.

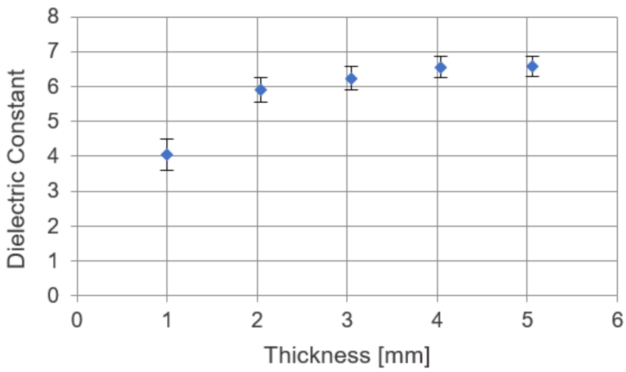

Fig 2. Dielectric constant vs thickness for 3D printed TPU.

Figure 2 shows the average of the measured dielectric constant for each type of sample according to its thickness. The measured value for the samples of 1 mm thickness is inconsistent with values reported at higher thicknesses. This is likely due to the sample being very thin at 1 mm and printed with 0.2 mm thick layers. The percentage of overall air in the measurement volume compared to material was greater, likely off-setting the results. It is important to mention that all the samples were printed with an infill of 100%. However, as in all FDM 3D printing processes peaks and valleys are visible in the samples. The surface roughness was analyzed further in the results section. The results are approximately constant for samples with a thickness from 2 mm to 5 mm. This stable trend provides reliability in the results obtained, concluding that the value of the dielectric constant for this type of printed material is approximately 6.32 ± 0.30.

4.2. Applied Pre-strain

Pre-straining dielectric EAPs has been demonstrated to enhance their actuation potential [14]. An iris stretcher machine, which uniformly expands the material omnidirectionally, was used to stretch the dielectric films and measure the maximum percentage of elongation achievable. The machine applies a uniform multi-directional load to round specimens in order to mechanically pre-strain the materials which increases actuation potential [15].

Ten samples were 3D printed with a circular shape (100 mm diameter and 0.2 mm thickness) with an external ring (15 mm of width and 0.8 mm of thickness) to prevent premature breaking and stress concentration in the clamped points. Clamping points were needed to mount the dielectric material on an iris stretcher for application of uniform planar pre-strain. These samples are depicted in Figure 3 prior to being stretched.

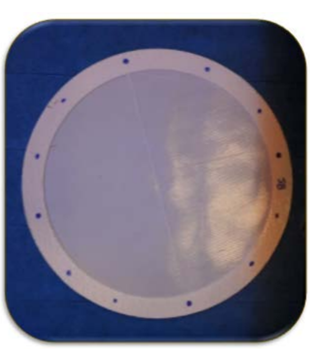

Fig 3. 3D Printed Dielectric material using fused deposition modeling (FDM).

Holes were punched at 12 points located in the external ring in order to allow for clamping to each arm of the machine. Then, the samples were stretched uniformly in planar directions. Results demonstrated that the dielectric films can achieve a maximum elongation of 560 ± 10% in the planar directions before failure, which refers to the area strain. Figure 4 shows the initial state of the sample when is clamped to the iris stretcher and, the final state once the sample was stretched at the maximum elongation.

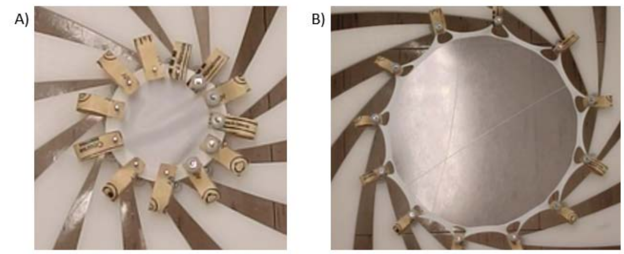

Fig 4. Elongations test a). Before stretch b). After stretch (elongation of 560%) [16].

4.3. Tensile properties

The orientation of the printing angle and the number of layers (thickness) are critical parameters when 3D printed parts are exposed to external loads. These two factors affect the mechanical properties of the material once it is printed. Tensile tests were carried out to characterize the mechanical properties of the material and the influence of the printing angle and number of layers. The samples were 3D printed and tested according to the dimensions and experimental procedure established in the "Standard Test Methods for tensile Properties" ASTM D638 – 14 [17].

Three different printing angles were tested: 0°, 45° and 90°, based on the direction of the applied external force. Figure 5 shows a representation of the three printing angles. In addition, five different thickness were tested varying the number of layers, from one layer (thickness of 0.20 ± 0.02 mm) to five layers (thickness of 1.00 ± 0.02 mm). Eight samples per printing angle for each different thickness were tested, for a total of 120 samples tested). The specimens were type IV, based on the ASTM D638 - 14 norm, generally used when direct comparison is required between materials in different rigidity cases.

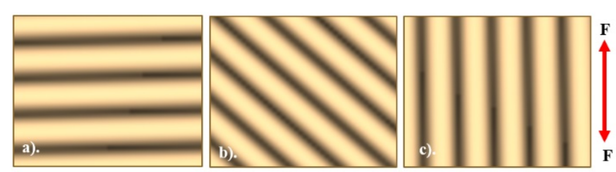

Fig 5. Printing angles: a) 90°; b) 45°; c) 0°.

A Mechanical Testing System (MTS Criterion - Model C45.605), universal loading machine was used to conduct the tensile testing, using a load cell of 1 kN. The MTS wedge grips were displaced at a rate of 50 mm/min with data collected at 100 Hz. The key specifications of the specimens tested for tensile test are described in the following tables.

Table 1
Key data of the Tensile Test – One-layer specimens

	Specimens - One Layer (Thickness: 0.2 mm)				
Angle	Number of Samples	Peak Load (SD) [N]	Peak Stress (SD) [MPa]	Strain at Break (SD) [mm/mm]	Young's Modulus (SD) [MPa]
90°	8	44.38 (2.38)	9.48 (0.65)	5.11 (0.42)	6.21 (0.61)
45°	8	82.47 (2.25)	14.94 (0.63)	8.39 (0.49)	3.56 (0.58)
0°	8	135.12 (2.66)	26.56 (0.55)	9.31 (0.45)	3.04 (0.60)

Table 2
Key data of the Tensile Test – Two-layer specimens

Specimens - Two Layers (Thickness: 0.4 mm)					
Angle	Number of Samples	Peak Load (SD) [N]	Peak Stress (SD) [MPa]	Strain at Break (SD) [mm/mm]	Young's Modulus (SD) [MPa]
90°	8	53.28 (2.51)	11.22 (0.61)	4.91 (0.43)	6.78 (0.63)
45°	8	107.93 (2.35)	21.42 (0.57)	8.01 (0.47)	3.87 (0.60)
0°	8	143.03 (2.29)	28.16 (0.60)	8.64 (0.46)	3.29 (0.62)

Table 3
Key data of the Tensile Test – Three-layer specimens

Specimens - Three Layers (Thickness: 0.6 mm)					
Angle	Number of Samples	Peak Load (SD) [N]	Peak Stress (SD) [MPa]	Strain at Break (SD) [mm/mm]	Young's Modulus (SD) [MPa]
90°	8	69.25 (2.24)	13.85 (0.62)	4.62 (0.47)	7.22 (0.58)
45°	8	127.64 (2.28)	25.94 (0.63)	7.38 (0.42)	4.13 (0.60)
0°	8	155.55 (2.41)	30.91 (0.67)	8.29 (0.40)	3.51 (0.55)

Table 4
Key data of the Tensile Test – Four-layer specimens

Specimens - Four Layers (Thickness: 0.8 mm)					
Angle	Number of Samples	Peak Load (SD) [N]	Peak Stress (SD) [MPa]	Strain at Break (SD) [mm/mm]	Young's Modulus (SD) [MPa]
90°	8	76.94 (2.33)	15.14 (0.61)	4.38 (0.44)	7.85 (0.59)
45°	8	138.66 (2.53)	27.68 (0.55)	6.59 (0.40)	4.28 (0.62)
0°	8	170.21 (2.44)	33.44 (0.62)	7.14 (0.42)	3.64 (0.66)

Table 5
Key data of the Tensile Test – Five-layer specimens

Specimens - Five Layers (Thickness: 1 mm)					
Angle	Number of Samples	Peak Load (SD) [N]	Peak Stress (SD) [MPa]	Strain at Break (SD) [mm/mm]	Young's Modulus (SD) [MPa]
90°	8	96.47 (2.40)	18.69 (0.67)	4.25 (0.41)	8.14 (0.54)
45°	8	159.11 (2.11)	31.57 (0.56)	6.18 (0.46)	4.46 (0.59)
0°	8	178.24 (2.38)	35.32 (0.61)	6.60 (0.41)	3.72 (0.60)

The samples present different responses depending of the printing angle and thickness. An angle of 0° means that the infill of the sample has a parallel orientation compared to the load direction. These types of samples are more resistant to loads and present the highest load peaks and greatest deformations when compared to the samples with a perpendicular infill orientation.

The number of layers of the samples affects the mechanical response to external loads. The samples with five layers presented higher stress and lower strains, making the samples harder to stretch. The more material the sample has, the greater the rigidity it presents when is exposed to external loads.

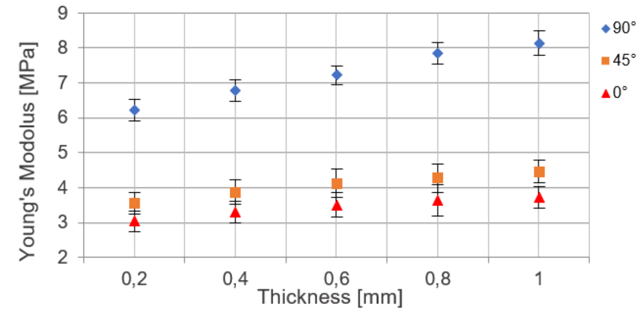

Fig 6. Young´s modulus vs Thickness for TPU samples with different printing angles.

Figure 6 shows the average value obtained for the Young's modulus based on the results of the 8 samples tested, for each type of sample configuration. Based on the previous results, it is possible to identify a similar response between the samples with 0° and 45°. These types of samples present a similar tendency when the thickness is increased, having an increment in the Young's modulus of approximately 1 MPa. On the other hand, the samples printed at 90° present higher values, almost double compared to the other sample types, and present an increment in the Young's modulus of approximately 2 MPa. It is important to mention that in the analysis of this experimental test a perfect polymerization is assumed, which means that each line of impression is perfectly joined to the others as well as each printing layer.

4.4. Pre-strain

One important concern associated with the use of electro active materials is the required pre-strain to improve the overall performance of the active structure. When a pre-strain is applied to a polymer film the polymer chains are aligned in the plane of the film and the thickness of the film is decreased. The pre-strain enhances the dielectric breakdown of the elastomer films and realigns defects that could be responsible for premature dielectric breakdown [18]. However, the pre-strain affects the mechanical properties of the elastomer film reducing the elastic energy density due to the cyclic stress concentration and creep effect.

Elastomeric materials are desired as dielectric films because these materials present high viscoelasticity and weak intermolecular forces, making the material flexible and easy to stretch. The most important characteristic of elastomers is the elastic recovery after deformation. In addition, when an elastomeric material is pre-strained, it can reach a regime where a small range of stress can achieve a large deformation [18].

Fifteen dielectric electroactive actuators were made (5 per each pre-strain percentage: 63%, 360% and 560%), using 3D printed TPU as the dielectric material and carbon grease for the electrodes, varying the pre-strain in the dielectric film to determine the percentage of pre-strain best suited to obtain a better response of the electroactive structure. All the samples were printed using a path of concentric circles and consisted of one printed layer. The actuators were tested using a high voltage supply (TREK 610E), increasing the voltage gradually between 0 and 10 kV dc until the structure reached voltage breakdown. The current was limited to a maximum of 2000 µA. Figure 7 shows the average voltage breakdown of the samples in relation to each pre-strain percentage.

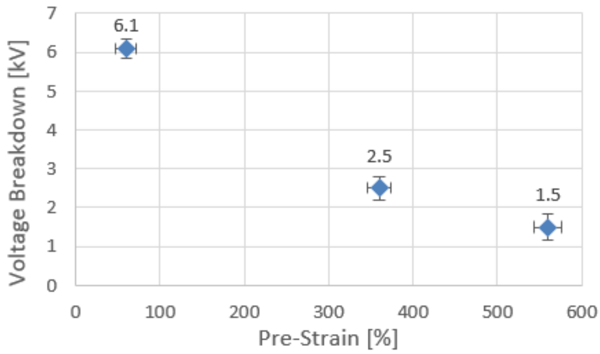

Fig 7. The pre-strain effect on the voltage breakdown.

Figure 7 above, depicts how the pre-strain affects the voltage breakdown of the material. An excessive percentage of pre-strain affects the resistance to support an electric field. This could happen at high pre-strains, because the thickness of the elastomer film is reduced significantly, to only a few microns, making the material reach its elastic limits faster and affecting its resistance to electric fields. Figure 8 shows the electrically induced deformation of the membrane as a function of its pre-strain.

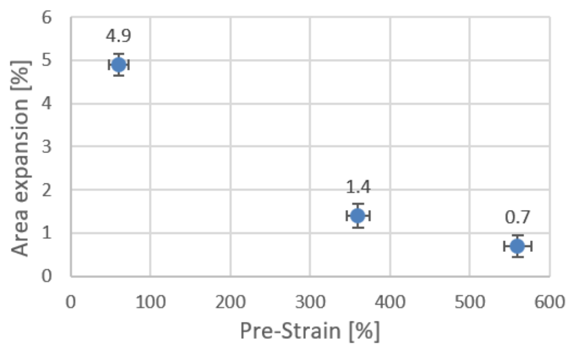

Fig 8. The pre-strain effect on the actuation.

From the tested values, at approximately 63% of pre-strain the electroactive structure increases its resistance to voltage, making this value adequate to improve the performance of the structure. Although, it is known that dielectric strength increases with the pre-strain of a dielectric elastomer, in this case low pre-strain improves the resistance of the dielectric elastomer to voltage application. This is likely due to the manufacturing process. High pre-strain could cause imperfections like holes, valleys and airgaps, which are common in 3D printed structures and can form from stress concentrations from manufacturing imperfections. These amplified imperfections in turn cause reduction in the voltage breakdown strength.

4.5. Surface metrology

3D printers that utilize FDM technology build parts layer by layer by heating thermoplastic material to a semi-liquid state and extruding it according to computer-controlled paths. One of the most significant disadvantages of FDM is its high surface roughness, especially if compared to other manufacturing processes. A precise characterization of roughness and surface topography is of prime importance for these types of actuators to ensure that the surface integrity of the dielectric 3D printed material responds properly to mechanical loads and electric fields [19].

Two types of dielectric 3D printed films were characterized. The first was made using a 3D printing path based on concentric circles, while the other type was made using a 3D printing path based on parallel lines. The printed samples have exactly the same dimensions and were printed with the same settings (speed: 10 mm/s, temperature: 205°C, nozzle diameter: 0.4 mm, bed temperature: 60°C). The printing time for the samples with the concentric circles path was 28 minutes, and the printing time for the samples with the parallel lines path was 35 minutes. Five samples for each type of 3D printing path were considered, for a total of 10 samples characterized.

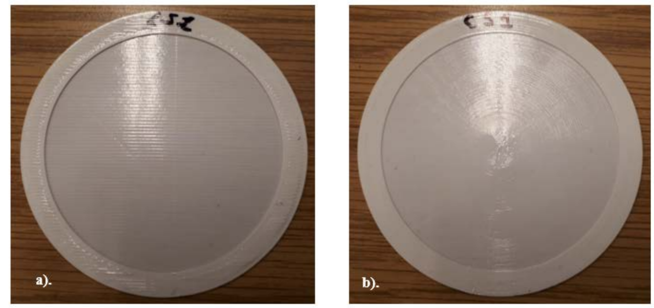

Fig 9. Dielectric 3D printed films: a). Line path; b). Concentric circles path.

The samples were measured using an optical microscope "Bruker Contour Elite K 3D", utilizing green light interferometry and an optical magnification of 10X/0.30. An approximate area of 18 mm² was scanned for the samples with line paths, and an approximate area of 33 mm² was scanned for the samples with concentric circles path, in order to make more visible the curvature of this type of path. The equipment was able to capture more than 95% of all data for each sample measured.

4.5.1. Concentric circles path

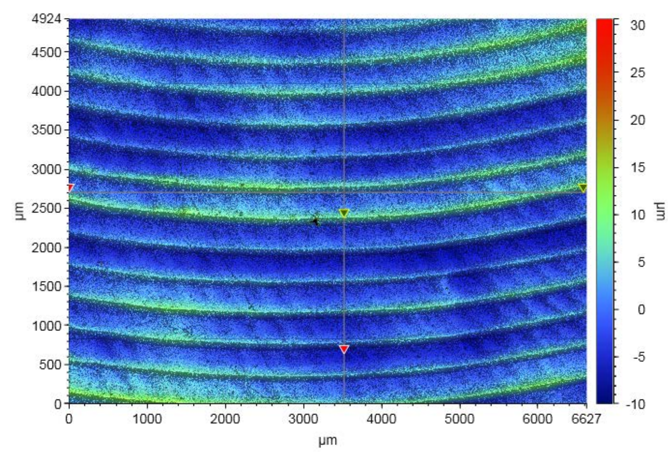

Fig 10. 2D surface of 3D printed TPU using concentric circles path.

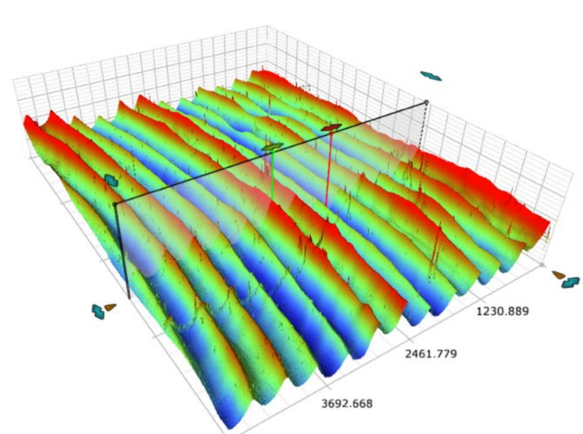

Fig 11. 3D Contour of 3D printed TPU using concentric circles path.

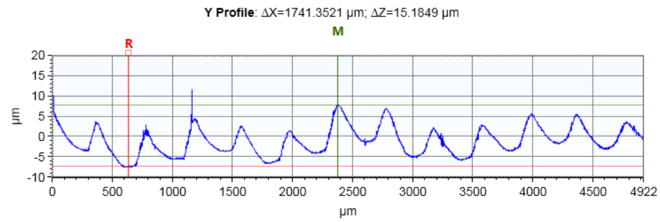

Fig 12. Roughness plot of a 3D printed TPU using concentric circles path.

4.5.1. Line path

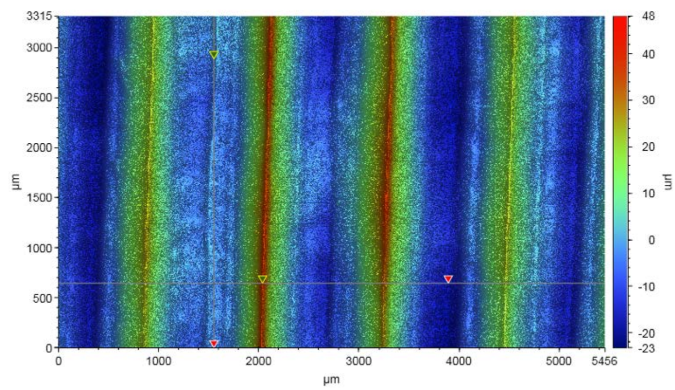

Fig 13. 2D surface of 3D printed TPU using line path.

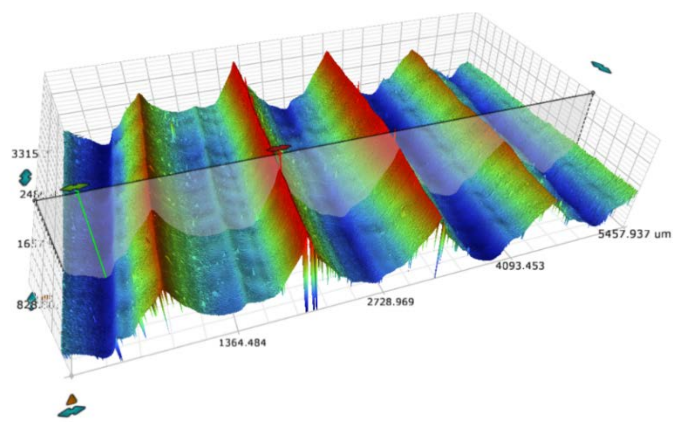

Fig 14. 3D Contour of 3D printed TPU using line path.

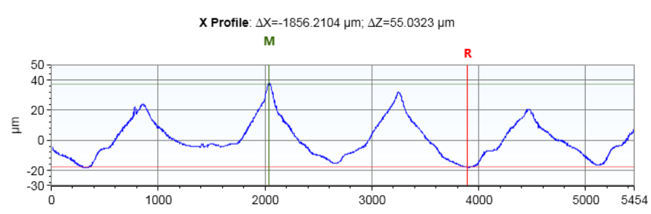

Fig 15. Roughness plot of a 3D printed TPU using line path.

The images shown above display the surface characteristics of the samples printed, using different paths in the movement of the printer head. Both in 2D and 3D images it is possible to see surfaces without holes, or discontinuities that may affect the structure of the dielectric film. On the other hand, it can be observed that both samples have a cyclic topography described by peaks and valleys with approximately the same distances between them. However, not all peaks and valleys are at the same height, this "randomness" is a feature of FDM 3D printing. The samples with the concentric circles path present in average a ΔZ (difference between the maximum peak and the minimum valley) of 15.63 µm, while the samples with line path present an average ΔZ of 56.41 µm demonstrating the concentric circles have a tighter z axis tolerance. The samples with concentric circles present a relatively smoother surface due to the continuity of the process. For the concentric circle samples, the printing head follows a continuous path with constant velocity, while for the line samples the printing head needs to change the travel direction multiple times. This produces a process with more changes in acceleration and velocity, creating a greater variability in the surface roughness.

4.6. Actuation

The samples for the actuation test were 3D printed with the same dimension and printing settings as in the surface metrology test. The DEAP actuators were made using TPU as the dielectric material and carbon conductive grease (MG Chemicals® #846) as the electrode material. The electrodes were painted on both sides of the dielectric film in a circular shape with a diameter of 50 mm. Conductive copper tape was used to connect the electrodes to the high voltage supply. The dielectric films were stretched until they reached a pre-strain of 63% using the same machine used for the pre-strain test.

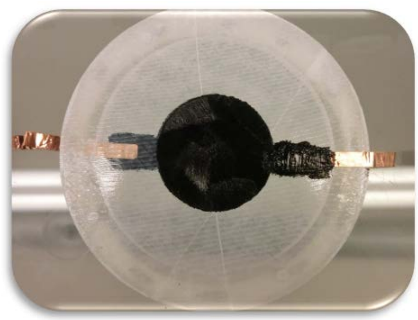

Fig 16. Dielectric electroactive polymer actuator structure

Ten electroactive structures were analyzed, five per each type of 3D printing path, under the same manufacturing process to validate consistency and replicability based on the actuation behavior. The maximum percentage of expansion of the active area (equivalent to the area of the electrodes) was analyzed with respect of the voltage breakdown. The value of the area expansion percentage is taken when the structure presents the maximum deformation just before the rupture of the dielectric film by the electric field. The area expansion for the samples with line path were measured in two directions: when the printed lines are parallel to the deformation direction, and when the printed lines are perpendicular to the deformation direction.

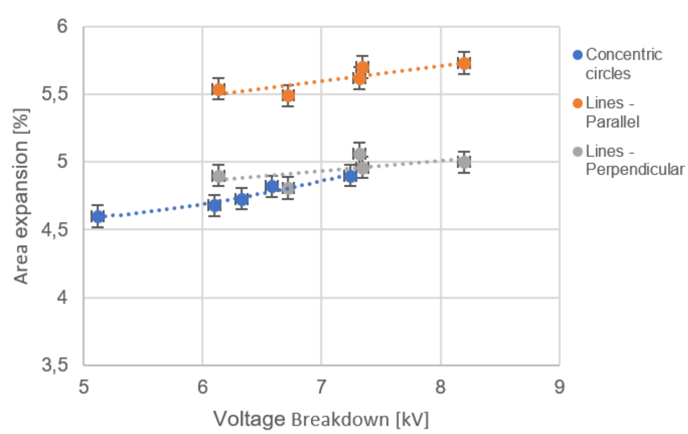

Fig 17. Area expansion of the dielectric electroactive actuators.

Based on figure 17, it is possible to conclude that the printing path affects the performance of the electroactive structures. Each type of DEAP actuator presents a consistent actuation response proving that the manufacturing process is replicable. The average expansion area percentage of the electroactive actuators with the concentric circles path was 4.73%. The average expansion area percentage of the electro active actuators with line path was 5.71% in the parallel direction, and 4.91% in the perpendicular direction. All the actuators presented deformations visible to the human eye, and were able to support voltages between 5.1 and 8.2 kV. It is important to mention that in many occasions these types of structures present deformation in the micro scale. Figures 18, 19 and 20 show the video analysis of the actuation distance in mm of one sample using an open source software, "Tracker". Tracker is a free video analysis software capable of calculating deformations. The Tracker tool extends traditional video analysis by enabling users to create particle models based on Newton's law. In a typical video modeling experiment the user captures and opens a digital video file, calibrates the scale (based on image distance in pixels between two points), and defines appropriate coordinate axes to analyze the displacement of a certain point [20].

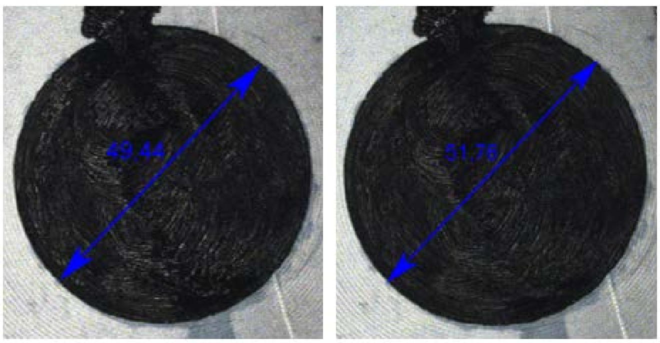

Fig 18. Actuation of 3D printed dielectric EAP actuator using concentric circles path at 4.67 kV.

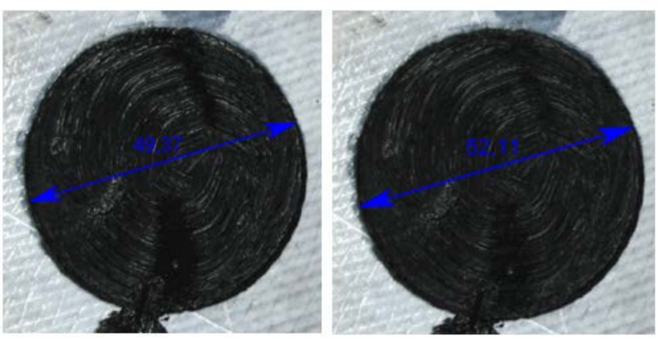

Fig 19. Actuation of 3D printed dielectric EAP actuator using line path – Parallel direction at 5.73 kV.

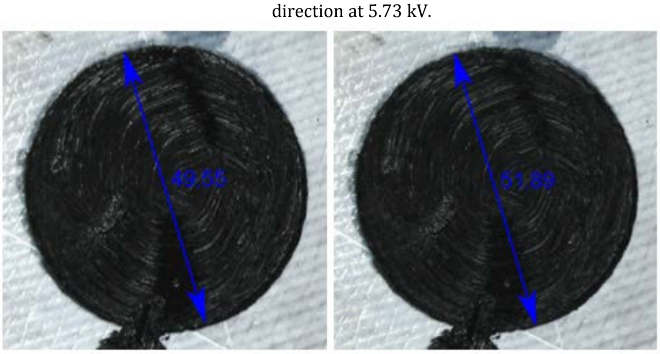

Fig 20. Actuation of 3D printed dielectric EAP actuator using line path – Perpendicular direction at 5.02 kV.

5. Conclusions

A novel design of a 3D printed dielectric electroactive actuator was presented. The manufacturing process uses 3D printing to produce dielectric films. The electromechanical properties of these types of films were characterized. The dielectric material has a high dielectric constant, when compared with other polymeric materials, making this material suitable for electroactive structures. Similarly, the dielectric material has excellent elongation properties.

Through tensile testing it was possible to analyze the characteristic behavior of the material under external loads, providing evidence of the importance of pre-strain in this type of electroactive structure. Pre-straining the material allows the electroactive structure to present greater deformations with smaller stresses in its zone of elastic behavior. The influence of the printing angle and thickness of the dielectric material were analyzed, finding that the resistance of the material to external loads and electric fields depends on the orientation in which it is printed and the number of layers. The surface of the 3D printed samples was also characterized, concluding that dielectric films have a characteristic roughness which depends on the type of path used in the printing. Concentric circle pathways provide a tighter z-axis tolerance compared to line based pathways, by approximately 30 microns. The surface of the printed samples has a cyclic topography described by peaks and valleys with approximately the same distance between them.

As expected, the performance of the dielectric electroactive actuators is dependent on the printing angle which is defined by the printing path. Based on the tensile and actuation tests, it is possible to validate how the orientation modifies the resistance of the material, affecting its performance as an actuator. However, this feature of 3D printing can be used as an advantage, making it possible to control the preferential directions of actuation.

This paper studied the elastic behavior of TPU using 3D printing as the manufacturing process and showed TPU has optimal properties for a dielectric electroactive structure. However, improvements to the material can be made through reduction in surface defects, alternate pre-strain methods such as chemical processes, and enhancement of the material's dielectric constant through addition of additives. The future goal of this work is to create a fully 3D printable electroactive polymer structure, simplifying the manufacturing process and expanding the geometric designs capable with these structures.

The manufacturing process demonstrates replicability of the electroactive structures, obtaining similar actuation responses based on different printing paths tested in this study. 3D printing of dielectric elastomers for use as electroactive polymers using FDM as the principal technique was successfully demonstrated and opens the possibility to print the entire structure in just one process.

Acknowledgments

This work was sponsored in part by the National Science Foundation under grant CNS-1726865. We thank Dr. Yung C. Shin (professor of mechanical engineering at Purdue University) and his graduated student Gaurav Vilas, who provided insight and expertise in the surface metrology subject.

References

[1] Bar-Cohen, Y.; Cardoso, V. F.; Ribeiro, C.; Lanceros-Méndez, S. Electroactive Polymers as Actuators. In Advanced Piezoelectric Materials; Elsevier, 2017; pp 319–352. https://doi.org/10.1016/B978-0-08-102135-4.00008-4.

[2] Prahlad, H.; Kornbluh, R.; Pelrine, R.; Stanford, S.; Eckerle, J.; Oh, S. Polymer Power: Dielectric Elastomers and Their Applications in Distributed Actuation and Power Generation; Proceedings of ISSS: Bangalore, India, 2005; Vol. 13, p 8.

[3] Biddiss, E.; Chau, T. Dielectric Elastomers as Actuators for Upper Limb Prosthetics: Challenges and Opportunities. Med. Eng. Phys. 2008, 30 (4), 403–418.

[4] Pelrine, R.; Kornbluh, R.; Joseph, J.; Heydt, R.; Pei, Q.; Chiba, S. High-Field Deformation of Elastomeric Dielectrics for Actuators. Mater. Sci. Eng. C 2000, 11 (2), 89–100. https://doi.org/10.1016/S0928-4931(00)00128-4.

[5] Cardoso, V. F.; Ribeiro, C.; Lanceros-Mendez, S. Metamorphic Biomaterials. In Bioinspired Materials for Medical Applications; Elsevier, 2017; pp 69–99.

[6] Kovacs, G.; Düring, L.; Michel, S.; Terrasi, G. Stacked Dielectric Elastomer Actuator for Tensile Force Transmission. Sens. Actuators Phys. 2009, 155 (2), 299–307. https://doi.org/10.1016/j.sna.2009.08.027.

[7] Mohd Ghazali, F. A.; Mah, C. K.; AbuZaiter, A.; Chee, P. S.; Mohamed Ali, M. S. Soft Dielectric Elastomer Actuator for Micropump Application. Sens. Actuators Phys. 2017, 263, 276–284. https://doi.org/10.1016/j.sna.2017.06.018.

[8] Kornbluh, R. Fundamental Configurations for Dielectric Elastomer Actuators.

In Dielectric Elastomers as Electromechanical Transducers; Elsevier, 2008; pp 79–90. https://doi.org/10.1016/B978-0-08-047488-5.00008-3.
[9] Schlaak, H. F.; Lotz, P.; Matysek, M. Multistack Contractile Actuators. In Dielectric Elastomers as Electromechanical Transducers; Elsevier, 2008; pp 109–122. https://doi.org/10.1016/B978-0-08-047488-5.00011-3.
[10] Covestro AG. Innovative material properties. https://www.tpu.covestro.com/en/Technologies/Properties/Electrical-Properties (accessed 15 Jan 2019).
[11] Diabase Engineering (2018) X60 Ultra Flexible Filament. https://flexionextruder.com/shop/x60-ultra-flexible-filament-white/ (accessed 15 Jan 2019).
[12] Keysight Technologies (2016) Solution for measuring permittivity and permeability with LCR meters and impedance analyzers. http://literature.cdn.keysight.com/litweb/pdf/5980-2862EN.pdf (accessed 15 Jan 2019).
[13] D09 Committee. Test Methods for AC Loss Characteristics and Permittivity (Dielectric Constant) of Solid Electrical Insulation; ASTM International. https://doi.org/10.1520/D0150-18.
[14] Pelrine, R. High-Speed Electrically Actuated Elastomers with Strain Greater Than 100%. Science 2000, 287 (5454), 836–839. https://doi.org/10.1126/science.287.5454.836.
[15] Romo-Estrada, J.A., Newell, B. and Garcia, J., 2018, September. Mechanical Iris Stretcher for Electroactive Polymers. In ASME 2018 Conference on Smart Materials, Adaptive Structures and Intelligent Systems (pp. V002T02A002-V002T02A002). American Society of Mechanical Engineers.
[16] Gonzalez, D., Newell, B., Garcia, J., Noble, L. and Mamer, T., 2018, September. 3-D Printing of Dielectric Electroactive Polymer Actuators and Characterization of Dielectric Flexible Materials. In ASME 2018 Conference on Smart Materials, Adaptive Structures and Intelligent Systems (pp. V002T02A006-V002T02A006). American Society of Mechanical Engineers.
[17] D20 Committee. Test Method for Tensile Properties of Plastics; ASTM International. https://doi.org/10.1520/D0638-14.
[18] Ha, S. M.; Yuan, W.; Pei, Q.; Pelrine, R.; Stanford, S. Interpenetrating Networks of Elastomers Exhibiting 300% Electrically-Induced Area Strain. Smart Mater. Struct. 2007, 16 (2), S280–S287. https://doi.org/10.1088/0964-1726/16/2/S12.
[19] Araromi, O. A.; Conn, A. T.; Ling, C. S.; Rossiter, J. M.; Vaidyanathan, R.; Burgess, S. C. Spray Deposited Multilayered Dielectric Elastomer Actuators. Sens. Actuators Phys. 2011, 167 (2), 459–467. https://doi.org/10.1016/j.sna.2011.03.004.
[20] Software Tracker - Video analysis and modeling tool V.5.0.6. Douglas Brown. https://physlets.org/tracker/ (accessed 15 Jan 2019)